

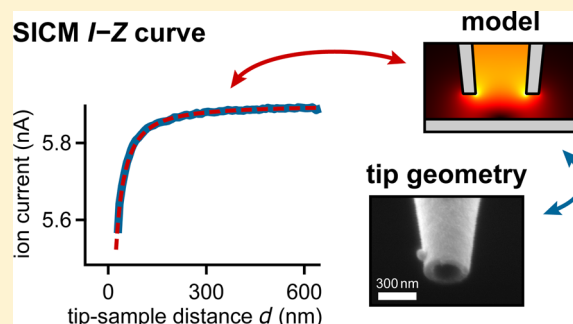
An Accurate Model for the Ion Current–Distance Behavior in Scanning Ion Conductance Microscopy Allows for Calibration of Pipet Tip Geometry and Tip–Sample Distance

Johannes Rheinlaender*¹ and Tilman E. Schäffer*¹

Institute of Applied Physics, University of Tübingen, Auf der Morgenstelle 10, 72076 Tübingen, Germany

Supporting Information

ABSTRACT: The scanning ion conductance microscope (SICM) is an emerging tool for noncontact topography imaging and multi-physical investigation of soft samples in aqueous environments such as living cells. Despite the increasing popularity of SICM, several aspects of the imaging process are still unknown; for example, there is still no accurate description of the behavior of the ion current for a varying tip–sample distance. To predict this ion current–distance behavior, we provide a new numerical model based on finite element modeling. The model allows, for the first time, accurately determining the tip–sample distance during an SICM experiment. Furthermore, we present a nondestructive method for calibrating the pipet tip geometry by fitting the numerical model to the experimental ion current–distance data and verify this method using pipets with opening radii between 30 and 300 nm.



INTRODUCTION

The scanning ion conductance microscope¹ (SICM) is an emerging scanning probe microscope especially suited for imaging the topography of delicate, soft samples such as living cells^{2–4} or suspended membranes,⁵ providing nanometer spatial resolution.^{6,7} In addition to topography imaging, the SICM has also been used for advanced nanopipet-based techniques, such as patch-clamping,⁸ molecule⁹ or liquid^{10,11} delivery, pipet-based electrochemistry,^{12,13} and mechanically stimulating^{14,15} or probing the sample.^{16–20}

An important imaging parameter that is usually not known during imaging is the tip–sample distance. The tip–sample distance may be estimated from recording the ion current vs the vertical tip position (“*I*–*Z* curve”), but this requires an accurate model of the ion current–distance behavior. The analytical model by Nitz et al.,²¹ although widely used today, has not yet been quantitatively verified. Another model, originally developed for the scanning electrochemical microscope (SECM) by Mirkin et al.²² based on numerical data,²³ was first adapted by Edwards et al.²⁴ for SICM and further improved recently by Wang et al.²⁵ by using data^{26,27} for more realistic geometries. We found that both models significantly deviate from the experimental data.

Despite the increasing popularity of the SICM, there is no nondestructive method for accurately quantifying the pipet geometry, which is the most important determinant for image resolution and detection sensitivity.^{6,28–31} The geometry of the pipet tip can be approximated by means of three parameters: the inner opening radius r_i , the outer opening radius r_o , and the inner half cone angle α . Different methods to determine these parameters have been published. For example, a pipet can be

metalized and imaged by scanning electron microscopy (SEM).³² However, this is a time-consuming procedure, and the metalized pipet might be impaired for SICM use afterward. Transmission electron microscopy (TEM) allows imaging of nonmetalized pipets^{33,34} but is also quite elaborate. In many SICM studies, r_i is estimated from the pipet’s electrical resistance by measuring the ion current through the pipet.³⁵ However, this method requires a separate estimate for α ,³⁶ which can easily vary by a factor of 2 even for pipets from an identical pulling procedure,^{32,37} resulting in a large error for r_i . Other methods that were recently introduced involve a quasi-controlled breakage of the pipet,^{37,38} atomic force microscope (AFM) combined with SICM,³⁹ or passage of nanoparticles through the pipet.⁴⁰ However, there is currently no method for a nondestructive determination of all three tip geometry parameters within a running SICM experiment.⁴¹

Here, we establish a new numerical model for the ion current–distance behavior in the SICM based on finite element modeling (FEM), which predicts the experimental data much more accurately than the previous models by Nitz et al. and Wang et al. We then present a nondestructive method for calibrating the pipet tip geometry based on fitting an experimental *I*–*Z* curve with the numerical model. Finally, we show how to determine the tip–sample distance from the ion current during an experiment.

Received: September 21, 2017

Accepted: October 10, 2017

Published: October 10, 2017

EXPERIMENTAL SECTION

SICM Setup. We used a home-built SICM head that was made compatible with a commercial AFM setup (for details, see ref 42). All SICM measurements were recorded at room temperature in phosphate-buffered saline as electrolyte with a conductivity of $\sigma = 1.58$ S/m at 25°C, as determined with a commercial conductivity meter (EL30, Mettler Toledo, Greifensee, Switzerland). The voltage between the electrodes was set to $V_0 = 100$ mV or 200 mV depending on the pipet size. By reversing the voltage, we routinely verified that no ion current rectification (ICR) effect⁴³ occurred. Data were recorded and analyzed using custom-written software in Igor Pro (WaveMetrics Inc., Lake Oswego, OR, USA).

Nanopipets. Nanopipets were fabricated from capillaries of either borosilicate glass (1B100F-4, World Precision Instruments Inc., Sarasota, FL, USA) or quartz glass (QF100-50-7.5, Sutter Instrument Company, Novato, CA, USA) using a commercial CO₂-laser-based micropipet puller (P-2000, Sutter Instruments, Novato, CA, USA). The pipet's inner opening radius r_i was between 30–300 nm, and the ratio of outer to inner opening radius r_o/r_i (see insets in Figure 1) was typically 1.5 ± 0.1 (average \pm standard deviation, see Figure S3a) as measured with SEM (see below). We verified that no mechanical contact between tip and sample occurred for the considered ion current levels by recording I – Z curves on an AFM cantilever^{18,44} before the experiments.

Scanning Electron Microscopy. After the SICM measurements, the pipets were washed three times with distilled water and sputter-coated (for high step coverage), together with their respective twin from pulling, with a 10 ± 5 nm thick layer of aluminum or gold. Then, they were imaged by SEM (Zeiss Gemini Supra 40, Carl Zeiss GmbH, Oberkochen, Germany; Philips XL30, Philips, Amsterdam, Netherlands) under an angle of 45° relative to the pipet axis. From the SEM images of the pipets or their respective unused (clean) twins (insets in Figure 1), the inner and outer opening radii, r_i and r_o , respectively, were determined (corrected for the aluminum or gold coating and with an estimated precision of 10%). The inner half cone angle, α , is not directly accessible in SEM images and has often been estimated from the outer cone angle of the pipet assuming a constant ratio of outer to inner pipet radius.³² However, because this assumption might not always be valid,^{37,41} we estimated α from r_i (from the SEM images) and from the electrical resistance of the pipet measured from the ion current at a large tip–sample distance [eq 3] (similar to ref 40 but for each pipet individually), thereby avoiding any artifacts from the cone angle determination.⁴¹ The pipet's cone angle was typically $3.3 \pm 0.9^\circ$ (average \pm standard deviation, see Figure S3b). In the case of a nonconical pipet, the estimated cone angle becomes an effective cone angle (see Figure S5 for details).

FEM Calculations. FEM calculations were performed as described previously.^{24,28} Briefly, for ion current vs distance behavior to be calculated, a finite element model of the tip region was designed in axial symmetry. The pipet (inner opening radius r_i , outer opening radius r_o , inner half cone angle α) was placed at a vertical distance d from a flat horizontal sample surface (Figure 2a, see Supporting Information and Figure S1 for details). The pipet walls and the sample surface were modeled as electrical insulators (because surface or “zeta” potentials are strongly shielded due to the short Debye length for the ion concentrations of the electrolytes typically used in

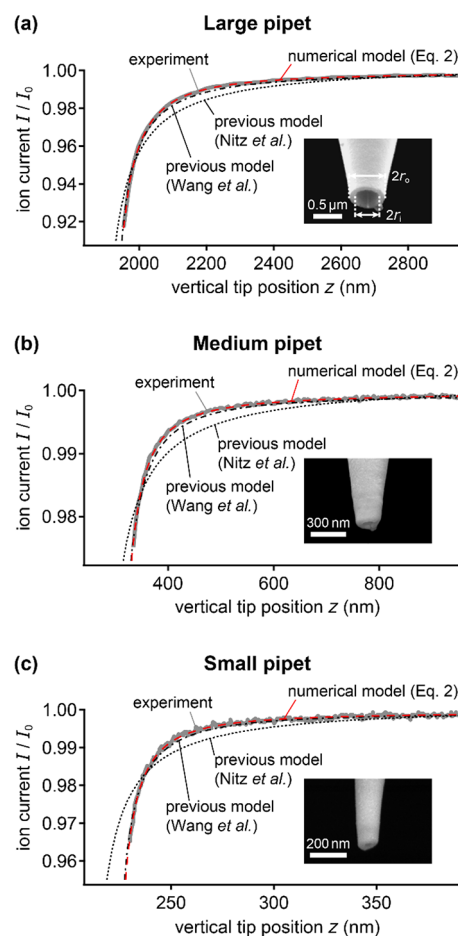


Figure 1. Experimental I – Z curves (continuous gray traces) for three pipets with different opening radii and comparison with the predictions from the numerical model based on FEM [dashed red trace, eq 2] and from the previous models by Nitz et al.²¹ (dotted gray trace) and Wang et al.²⁵ (dash-dotted gray trace). The insets show SEM images of the respective pipets at an angle of 45° relative to the pipet axis for the determination of inner (r_i) and outer (r_o) opening radii. (a) I – Z curve recorded with a large pipet manufactured from borosilicate glass ($r_i = 220 \pm 20$ nm, $r_o = 300 \pm 30$ nm $\cong 1.4r_i$, $\alpha = 3.5 \pm 0.3^\circ$, $I_0 = 12.8$ nA). (b) I – Z curve recorded with a medium-sized pipet manufactured from borosilicate glass ($r_i = 55 \pm 10$ nm, $r_o = 75 \pm 10$ nm $\cong 1.4r_i$, $\alpha = 3.2 \pm 0.3^\circ$, $I_0 = 2.9$ nA). (c) I – Z curve recorded with a small pipet manufactured from quartz glass ($r_i = 29 \pm 5$ nm, $r_o = 43 \pm 10$ nm $\cong 1.5r_i$, $\alpha = 1.9 \pm 0.3^\circ$, $I_0 = 950$ pA). The models were matched to the experimental data by offsetting the vertical tip positions and adjusting the saturation current I_0 .

SICM experiments supported by the fact that no ICR was observed). The ion current through the pipet was calculated by solving the Poisson equation in the electrolyte domain using commercial FEM software (COMSOL Multiphysics 4.1, COMSOL AB, Stockholm, Sweden).

RESULTS AND DISCUSSION

Experimental I – Z Curves. We moved a large ($r_i = 220$ nm), medium-sized ($r_i = 55$ nm), and small ($r_i = 29$ nm) nanopipet toward a flat glass surface and recorded the ion current I as a function of the vertical tip position z (“ I – Z curve”) (Figure 1). We ensured that no mechanical contact between tip and sample occurred (see Nanopipets section). Both the saturation current (I_0) and the shape of the I – Z curve were strongly dependent on the inner opening radius r_i . For

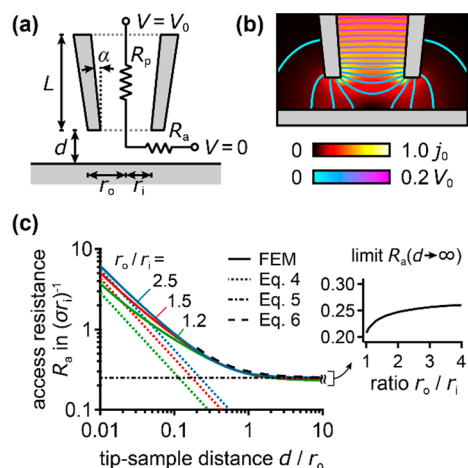


Figure 2. Numerical model for the ion current vs tip-sample distance behavior. (a) Schematic of the geometry and equivalent circuit for the ion current through the nanopipet. (b) Representative FEM calculation of the ion current density in the tip region (parameters: $r_o/r_i = 1.5$, $\alpha = 4^\circ$). The color scale is in units of $j_0 = I_0/(\pi r_i^2) \cong \sigma \tan(\alpha) V_0/r_i$. The contour lines show the electric potential V (in equally spaced intervals of $0.01V_0$). (c) Access resistance of the pipet vs tip-sample distance calculated with FEM for different values of the ratio r_o/r_i in comparison with the analytical limits [eqs 4 and 5] and to the “far field” approximation [eq 6]. The inset shows the limit access resistance $R_a(d \rightarrow \infty)$ as a function of r_o/r_i .

example, the vertical distance between the two positions, at which the current dropped to 99 and 98% of I_0 , respectively, was 120 nm for the large pipet (Figure 1a), 31 nm for the medium-sized pipet (Figure 1b), and 9 nm for the small pipet (Figure 1c).

After recording the I - Z curves, the geometric parameters (r_i , r_o , α) of the pipet tips were determined using SEM in combination with the saturation current I_0 (insets in Figure 1, see Scanning Electron Microscopy section for details). We then used these parameters to calculate I - Z curves with the models by Nitz et al.²¹ (Figure 1, dotted black traces) and Wang et al.²⁵ (Figure 1, dash-dotted black traces). To account for the unknown vertical position of the sample, which a priori is not known in the experiment, the calculated I - Z curves were matched to the experimental data by fitting with an offset z_0 in the vertical tip position, $z = z_0 + d$. It can be clearly seen that the predictions from these previous models systematically deviate from the experiment (maximum absolute deviation of the model by Nitz et al. 205, 31, and 11 pA and of that by Wang et al. 27, 5.6, and 2.7 pA for the large, medium-sized, and small pipets, respectively) and generally predict an ion current that is too small. In the case of the model by Wang et al., the deviation visually appears small but turns out to be significant later (see Results and Discussion, following sections).

Numerical Model. To obtain a more accurate prediction for the I - Z curves, we developed a new numerical model. To describe the total electrical resistance of the equivalent circuit for the ion current through the nanopipet (Figure 2a), we consider the resistance of the electrolyte in the pipet inner room, R_p , and the distance-dependent access resistance of the pipet opening, $R_a(d)$ (the resistances in the wires and in the electrodes are neglected). R_p is given by³⁵

$$R_p = \frac{1}{\pi \sigma r_i \tan \alpha} \quad (1)$$

which corresponds to eq 3 in ref 21 within the reasonable assumption $L \gg r_i$, i.e., that the length L of the conical part of the nanopipet is large compared to the pipet opening size. We used FEM to calculate the ion current through the tip region (Figure 2b) and the access resistance of the pipet opening $R_a(d)$ as a function of the tip-sample distance d for different values of the ratio of outer to inner opening radius, r_o/r_i , and pipet cone angle, α (see FEM Calculations section and Figure S1 for details). For the typical experimental small cone angles α , the functional form of $R_a(d)$ does not significantly depend on α (Figure S2a) but depends on r_o/r_i (Figure 2c). We therefore tabulated R_a as a function of d for different values of r_o/r_i [$R_a^{(r_o/r_i)}(d)$, Table S1]. The ion current can be then calculated from these tabulated values by

$$I(d) = \frac{V_0}{R_p + R_a^{(r_o/r_i)}(d)} = \frac{R_p + R_a^{(r_o/r_i)}(d \rightarrow \infty)}{R_p + R_a^{(r_o/r_i)}(d)} I_0 \quad (2)$$

with the saturation current³⁰

$$I_0 = I(d \rightarrow \infty) = \frac{V_0}{R_p + R_a^{(r_o/r_i)}(d \rightarrow \infty)} \cong \frac{\sigma V_0 r_i}{\frac{1}{\pi \tan \alpha} + \frac{1}{4}} \quad (3)$$

using eq 5. In the limit of small α , eq 3 approaches the frequently used formula $I_0 \approx \pi \sigma V_0 r_i \tan \alpha$.^{35,36} Compared to the new numerical model, the previous models by Nitz et al.²¹ and Wang et al.²⁵ predict a smaller ion current and flatter distance behavior (Figure S2b) and deviate by, for example, up to 67 and 9% in ion current, respectively, for $\alpha = 3^\circ$ and $r_o/r_i = 1.5$ (see Figure S2b).

To validate the new numerical model, we used eq 2 to calculate I - Z curves for the geometry parameters (r_i , r_o , α) of the pipets in Figure 1 (dashed red traces). A nearly perfect match between the numerical model and the experiment is achieved, and the deviations (7.7, 2.3, and 1.3 pA for the large, medium, and small pipets, respectively) are comparable to the noise of the measured ion current (approximately 5, 1, and 1 pA, respectively) and smaller than those of the previous models by Nitz et al. and Wang et al. This was the case for all 25 pipets used in this study (see Table S2). Therefore, eq 2 should be used in place of the previous models by Nitz et al. and Wang et al. (and Edwards et al.) because it provides a highly accurate and comprehensive description of the ion current as a function of the tip-sample distance.

Physical Interpretation. For the physical interpretation of the distance behavior, two extreme cases for the access resistance R_a are considered: In the case of a small tip-sample distance ($d \rightarrow 0$), the access resistance increases for decreasing d (Figure 2c, left part) and can be approximated by the resistance of the gap below the pipet walls²¹

$$R_a^{(r_o/r_i)}(d \rightarrow 0) = R_{\text{gap}}(d) = \frac{1}{\sigma} \frac{\ln(r_o/r_i)}{2\pi d} \quad (4)$$

(Figure 2c, dotted traces). In the case of a large tip-sample distance ($d \rightarrow \infty$), the access resistance approaches a constant level (Figure 2c, right part). This level only weakly depends on the ratio r_o/r_i and can be approximated by that of a circular pore of radius r_i facing an infinite half space^{45,46}

$$R_a^{(r_o/r_i)}(d \rightarrow \infty) \cong R_{\text{pore}} = \frac{1}{4\sigma r_i} \quad (5)$$

(Figure 2c, dash-dotted trace) for typical values of the ratio r_o/r_i (see Figure 2c, inset).³⁰

For intermediate and large tip-sample distances ($d/r_o \gtrsim 0.2$), the R_a curves roughly collapse on a single curve when plotted against the tip-sample distance in units of r_o (Figure 2c, middle part), showing that in this region the distance behavior of the access resistance depends not on the ratio r_o/r_i but on only r_o . In this region, the access resistance can be well approximated by the following semiempirical formula

$$R_a(r_o/r_i)(d \gtrsim 0.2r_o) \cong \frac{1}{4\sigma r_i} \left[1 + a \left(\frac{r_o}{d} \right)^b \right] \quad (6)$$

with $a \cong 0.2$ and $b \cong 1.2$ as dimensionless constants (Figure 2c, dashed trace). The ion current can be then approximated by

$$I(d \gtrsim 0.2r_o) \cong \frac{I_0}{1 + p/d^b} \quad (7)$$

with $p = a [4(\pi \tan \alpha)^{-1} + 1]^{-1} r_o^b$.

In conclusion, the distance behavior of the access resistance can be separated into two regions: a “near field” region ($d \lesssim 0.2r_o$), where it depends on the ratio r_o/r_i , and a “far field” region ($d \gtrsim 0.2r_o$), where it depends only on r_o . Note that at the distance separating the two regions, $d \cong 0.2r_o$, the access resistance is approximately $R_a(d = 0.2r_o) \cong 0.5(\sigma r_i)^{-1}$ and corresponds to a relative current drop of $[4(\pi \tan \alpha)^{-1} + 2]^{-1}$, which is typically a few % (for example, approximately 4% for the pipets used here with $\alpha \approx 3^\circ$).

Calibration of Pipet Tip Geometry from I - Z Curves. In the previous sections, we calculated I - Z curves for a given set of pipet tip geometry parameters (r_i , r_o , and α). Vice versa, the geometry parameters can be determined from the shape of the I - Z curve: Because of the distance dependence of the access resistance (see previous section), the shape of the I - Z curve at a small current drop (i.e., in the far field region) depends on only r_o and at a larger current drop (i.e., in the near field region) depends on the ratio r_o/r_i , whereas the saturation current depends on r_i and α [eq 3].

Accordingly, if the I - Z curve is recorded to a large current drop (i.e., to the near field), in our case more than $\sim 4\%$ (see previous section), all parameters can be determined independently (see Figure S4a). For example, fitting eq 2 with all geometry parameters free (not shown) gives $r_i = 220 \pm 10$ nm, $r_o = 320 \pm 10$ nm, and $\alpha = 3.5 \pm 0.1^\circ$ (fit parameter \pm estimated fitting error), matching the measured values (Figure 1a) within the estimated errors.

Recording an I - Z curve to a large current drop is, however, not always possible because mechanical contact between the pipet tip and the sample might then occur (see Nanopipets section for details), for example if the pipet opening is beveled (see Figure S6 for an investigation of that aspect). In the case of a smaller current drop (i.e., in the far field), in our case less than $\sim 4\%$, determining the three parameters (r_i , r_o , and α) independently is then not directly possible (see Figure S4b and c for the pipet in Figure 1b and c). To still determine the parameters (r_i , r_o , and α) also in this case, prior knowledge of one of the parameters or the ratio r_o/r_i is required. For our pipets, the ratio r_o/r_i was within a narrow range of $r_o/r_i = 1.5 \pm 0.1$ (average \pm standard deviation) (see Figure S3a). Fitting the I - Z curves in Figure 1 with eq 2 (not shown) then gives $r_i = 204 \pm 4$ nm, $r_o = 305 \pm 6$ nm, $\alpha = 3.8 \pm 0.1^\circ$ for the large pipet, $r_i = 44 \pm 1$ nm, $r_o = 65 \pm 2$ nm, $\alpha = 4.1 \pm 0.1^\circ$ for the medium pipet, and $r_i = 25 \pm 1$ nm, $r_o = 37 \pm 1$ nm, $\alpha = 2.3 \pm$

0.1° for the small pipet, in good agreement with the measured values. (In comparison, fitting the previous model by Wang et al. gives $r_i = 132 \pm 3$ nm, $r_o = 198 \pm 4$ nm, $\alpha = 6.1 \pm 0.1^\circ$ for the large pipet, $r_i = 29 \pm 1$ nm, $r_o = 44 \pm 1$ nm, $\alpha = 6.2 \pm 0.1^\circ$ for the medium pipet, and $r_i = 15 \pm 1$ nm, $r_o = 23 \pm 1$ nm, $\alpha = 3.8 \pm 0.1^\circ$ for the small pipet, which is about a factor of 2 off the measured value.) For proofing the reliability of the method for calibrating the pipet tip geometry from I - Z curves, the procedure was conducted with all 25 different pipets from seven different pipet pulling procedures with opening radii between 30 and 300 nm. The I - Z curves were recorded to an ion current drop of 2%, at which none of the pipets had contact with the sample. Afterward, the pipets were imaged using SEM. The I - Z curves were fit with eq 2 setting $r_o/r_i = 1.5$. The resulting values for r_i and r_o are in good agreement with the values from the SEM images, typically within the estimated error (Figure 3a). The resulting values for α varied slightly more than the radii but were also typically within the error bars (Figure 3b).

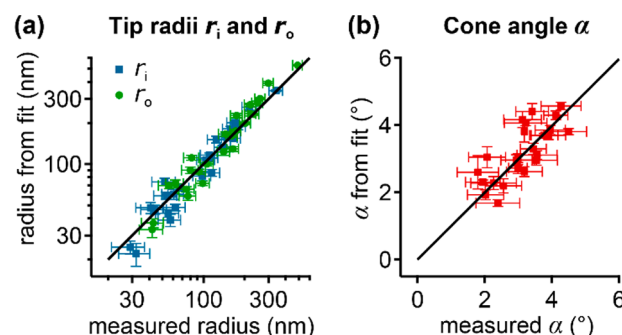


Figure 3. Comparison of tip geometry parameters, obtained by fitting the numerical model to experimental I - Z curves down to 2% current drop (assuming $r_o/r_i = 1.5$), with those measured with SEM for 25 pipets from seven different pipet pulling procedures. (a) Inner tip radius r_i and outer tip radius r_o from fit and measured with SEM. (b) Pipet cone angle α from fit and measured with SEM and I_0 (see Experimental Section for details). The horizontal error bars indicate the estimated error of the determination from the SEM images, and the vertical error bars indicate the estimated error of the fit. The bisecting line specifies perfect matches.

Calibration of Tip-Sample Distance. The absolute tip-sample distance is not directly accessible in SICM experiments because the vertical sample position is not known. If the pipet tip geometry is not known, the tip-sample distance can be obtained from an I - Z curve by a fit to one of our models using $d = z - z_0$ with z_0 as a free parameter. For example, fitting eq 2 [or, similarly, eq 7] to the I - Z curve in Figure 1a with all geometry parameters and z_0 as free fit parameters (not shown) gives $z_0 = 1930$ nm. From z_0 , we can then calculate the tip-sample distance as $d = z - z_0$. At 1% ion current drop, for example, the vertical tip position in Figure 1a is $z = 2210$ nm giving $d = 280$ nm.

If the pipet tip geometry is known (e.g., by using the method in the previous section), the new numerical model allows directly relating the ion current to the absolute tip-sample distance. The dependency is plotted in Figure 4 for selected, typical pipet geometries. For example, for the pipet in Figure 1a ($r_i = 204$ nm, $r_o = 305$ nm = $1.5r_i$, $\alpha = 3.8^\circ$), an ion current of $I = 0.99I_0$ (i.e., an ion current drop of 1%) corresponds to a tip-sample distance $d \approx 1.3r_i = 265 \pm 27$ nm (in agreement with the results from the previous paragraph). As a rule of thumb

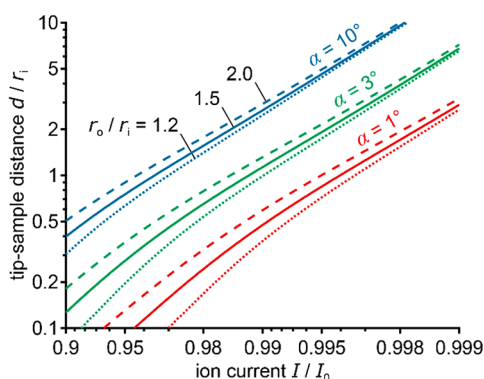


Figure 4. Calibration of the tip–sample distance from the ion current for different values of the ratio of outer to inner pipet opening radius, r_o/r_i , and for different values of the inner half cone angle α using the numerical model [eq 2 with Table S1].

that allows estimating the tip–sample distance from the measured ion current for typical SICM pipets ($r_o/r_i \approx 1.5$, $\alpha \approx 3^\circ$), an ion current drop of 10% ($I = 0.9I_0$) gives a tip–sample distance $d \approx 0.1r_i$, 1% gives $d \approx 1r_i$, and 0.1% gives $d \approx 10r_i$.²⁸

In the less frequently used AC mode,^{47,48} the vertical tip position is modulated sinusoidally, and the amplitude of the ion current, which depends on the tip–sample distance, is measured. The amplitude vs distance behavior can be deduced mathematically from the ion current vs distance behavior; however, care has to be taken when calculating amplitude and time-averaged ion current (see Figure S7 for details).

CONCLUSIONS

In this paper, an extensive analysis of the ion current vs distance behavior for the SICM is performed. We provide a new numerical model for the ion current as a function of the tip–sample distance based on FEM. We verify the model with experimental I – Z curves of pipets with known tip geometries. The new model predicts well the distance behavior, whereas two commonly used previous models^{21,25} significantly deviate from the experimental data. This is not surprising because these models use simplified assumptions: For example, Nitz et al.²¹ assume an unrealistic “mean course of the ions” reaching far down from the pipet opening, and FEM calculations show a high current density close to the pipet walls (Figure 2b). The analytical model adapted by Edwards et al.²⁴ was developed for SECM tips with a larger ratio of outer to inner radius^{22,23} compared to that of SICM pipets. However, even in the SECM model for smaller ratios,^{26,27} also recently used for nanopipets by Wang et al.,²⁵ the ion current close to the disklike SECM electrode is more homogeneously distributed than it is in a SICM pipet opening (Figure 2b). Therefore, these models generally overestimate the resistance (or underestimate the ion current) (see also Figure S2).

Our new numerical model now also allows calibrating two quantities that are usually not known in SICM experiments: the pipet tip geometry and the tip–sample distance. Using the new model, we present a nondestructive method for calibrating the pipet tip geometry (inner opening radius r_i , outer opening radius r_o , inner half cone angle α) based on the functional form of a measured I – Z curve. Note that the new numerical model [eq 2] has to be used for that, because neither the previous models nor our empirical approximation [eq 7] are accurate enough. The method can be applied within a running

experiment (and not only before or afterward) and can be implemented in every conventional SICM setup without any modification of the hardware. If the I – Z curve is recorded with a large current drop, the method provides all three geometry parameters. If the I – Z curve is recorded with only a small ion current drop, prior knowledge of one of the parameters or the ratio r_o/r_i is required. For our pipets, we found that the variation of the ratio of r_o/r_i was much smaller (7% here, see Figure S3a) than that of the inner half cone angle ($\sim 30\%$ here, see Figure S3b). Therefore, assuming a constant ratio r_o/r_i gives a notably more accurate calibration than assuming, as often done in the SICM community, a constant inner half cone angle. Note that the ratio r_o/r_i is naturally in a quite narrow range with an upper limit given by that of the original capillary³⁷ and a physical lower limit of 1.0. In contrast, the inner half cone angle can theoretically have any positive value below 90° .

Knowledge of the tip–sample distance will be useful for maintaining contact-free imaging,³⁰ for correcting for the effect of sample slope on SICM topography images,⁴⁹ or for quantifying hydrodynamic forces in mechanical SICM measurements.^{14–19} The new model for the distance behavior applies to all widely used SICM imaging modes: hopping/backstep mode^{29,50,51} and AC mode.^{47,48}

In summary, our new numerical model provides a quantitative base for a general understanding of the SICM measurement process and further allows for calibrating pipet tip geometry and tip–sample during a running SICM experiment.

ASSOCIATED CONTENT

Supporting Information

The Supporting Information is available free of charge on the ACS Publications website at DOI: 10.1021/acs.analchem.7b03871.

Finite element model and numerical model (Figure S1 and Figure S2), tabulated numerical model (Table S1), deviation models and experimental I – Z curve (Table S2), ratio of pipet opening radii vs cone angle (Figure S3), determination of geometry parameters by fitting I – Z curves (Figure S4), ion current vs distance behavior for nonideal pipet geometries (Figure S5 and Figure S6), and ion current and amplitude vs distance behavior and tip–sample distance in AC mode (Figure S7) (PDF)
Extended version of Table S1 as an Excel file (XLSX)
Extended version of Table S1 as ASCII text file (TXT)

AUTHOR INFORMATION

Corresponding Authors

*E-mail: johannes.rheinlaender@uni-tuebingen.de.

*E-mail: tilman.schaeffer@uni-tuebingen.de.

ORCID

Johannes Rheinlaender: 0000-0002-1976-9245

Tilman E. Schäffer: 0000-0001-5643-8384

Notes

The authors declare no competing financial interest.

ACKNOWLEDGMENTS

We thank Jan Seifert for discussions and Stefan Ballmann and Eva Lohmann for assistance with SEM imaging. We thank Asylum Research for technical support.

REFERENCES

- (1) Hansma, P. K.; Drake, B.; Marti, O.; Gould, S. A.; Prater, C. B. *Science* **1989**, *243*, 641–643.
- (2) Korchev, Y. E.; Bashford, C. L.; Milovanovic, M.; Vodyanoy, I.; Lab, M. J. *Biophys. J.* **1997**, *73*, 653–658.
- (3) Korchev, Y. E.; Gorelik, J.; Lab, M. J.; Sviderskaya, E. V.; Johnston, C. L.; Coombes, C. R.; Vodyanoy, I.; Edwards, C. R. *Biophys. J.* **2000**, *78*, 451–457.
- (4) Gorelik, J.; Shevchuk, A. I.; Frolenkov, G. I.; Diakonov, I. A.; Lab, M. J.; Kros, C. J.; Richardson, G. P.; Vodyanoy, I.; Edwards, C. R.; Klenerman, D.; Korchev, Y. E. *Proc. Natl. Acad. Sci. U. S. A.* **2003**, *100*, 5819–5822.
- (5) Böcker, M.; Muschter, S.; Schmitt, E. K.; Steinem, C.; Schäffer, T. E. *Langmuir* **2009**, *25*, 3022–3028.
- (6) Shevchuk, A. I.; Frolenkov, G. I.; Sánchez, D.; James, P. S.; Freedman, N.; Lab, M. J.; Jones, R.; Klenerman, D.; Korchev, Y. E. *Angew. Chem., Int. Ed.* **2006**, *45*, 2212–2216.
- (7) Rheinlaender, J.; Schäffer, T. E. *Anal. Chem.* **2015**, *87*, 7117–7124.
- (8) Gorelik, J.; Gu, Y.; Spohr, H. A.; Shevchuk, A. I.; Lab, M. J.; Harding, S. E.; Edwards, C. R.; Whitaker, M.; Moss, G. W.; Benton, D. C.; Sanchez, D.; Darszon, A.; Vodyanoy, I.; Klenerman, D.; Korchev, Y. E. *Biophys. J.* **2002**, *83*, 3296–3303.
- (9) Bruckbauer, A.; Ying, L. M.; Rothery, A. M.; Zhou, D.; Shevchuk, A. I.; Abell, C.; Korchev, Y. E.; Klenerman, D. *J. Am. Chem. Soc.* **2002**, *124*, 8810–8811.
- (10) Rodolfa, K. T.; Bruckbauer, A.; Zhou, D.; Shevchuk, A. I.; Korchev, Y. E.; Klenerman, D. *Nano Lett.* **2006**, *6*, 252–257.
- (11) Laforge, F. O.; Carpino, J.; Rotenberg, S. A.; Mirkin, M. V. *Proc. Natl. Acad. Sci. U. S. A.* **2007**, *104*, 11895–11900.
- (12) Zhang, H.; Wu, L.; Huang, F. J. *Vac. Sci. Technol., B: Microelectron. Process. Phenom.* **1999**, *17*, 269–272.
- (13) Morris, C. A.; Chen, C.-C.; Baker, L. A. *Analyst* **2012**, *137*, 2933–2938.
- (14) Sánchez, D.; Anand, U.; Gorelik, J.; Benham, C. D.; Bountra, D.; Lab, M. J.; Klenerman, D.; Birch, R.; Anand, P.; Korchev, Y. E. *J. Neurosci. Methods* **2007**, *159*, 26–34.
- (15) Pellegrino, M.; Orsini, P.; De Gregorio, F. *Neurosci. Res.* **2009**, *64*, 290–296.
- (16) Sánchez, D.; Johnson, N.; Li, C.; Novak, P.; Rheinlaender, J.; Zhang, Y.; Anand, U.; Anand, P.; Gorelik, J.; Frolenkov, G. I.; Benham, C.; Lab, M.; Ostanin, V. P.; Schäffer, T. E.; Klenerman, D.; Korchev, Y. E. *Biophys. J.* **2008**, *95*, 3017–3027.
- (17) Pellegrino, M.; Pellegrini, M.; Orsini, P.; Tognoni, E.; Ascoli, C.; Baschieri, P.; Dinelli, F. *Pfluegers Arch.* **2012**, *464*, 307–316.
- (18) Rheinlaender, J.; Schäffer, T. E. *Soft Matter* **2013**, *9*, 3230–3236.
- (19) Schäffer, T. E. *Anal. Chem.* **2013**, *85*, 6988–6994.
- (20) Clarke, R. W.; Novak, P.; Zhukov, A.; Tyler, E. J.; Cano-Jaimez, M.; Drews, A.; Richards, O.; Volynski, K. E.; Bishop, C.; Klenerman, D. *Soft Matter* **2016**, *12*, 7953–7958.
- (21) Nitz, H.; Kamp, J.; Fuchs, H. *Probe Microsc.* **1998**, *1*, 187–200.
- (22) Mirkin, M. V.; Fan, F.-R. F.; Bard, A. J. *J. Electroanal. Chem.* **1992**, *328*, 47–62.
- (23) Kwak, J.; Bard, A. J. *Anal. Chem.* **1989**, *61*, 1221–1227.
- (24) Edwards, M. A.; Williams, C. G.; Whitworth, A. L.; Unwin, P. R. *Anal. Chem.* **2009**, *81*, 4482–4492.
- (25) Wang, Y.; Cai, H.; Mirkin, M. V. *ChemElectroChem* **2015**, *2*, 343–347.
- (26) Amphlett, J. L.; Denuault, G. *J. Phys. Chem. B* **1998**, *102*, 9946–9951.
- (27) Cornut, R.; Lefrou, C. *J. Electroanal. Chem.* **2007**, *608*, 59–66.
- (28) Rheinlaender, J.; Schäffer, T. E. *J. Appl. Phys.* **2009**, *105*, 094905.
- (29) Novak, P.; Li, C.; Shevchuk, A. I.; Stepanyan, R.; Caldwell, M.; Hughes, S.; Smart, T. G.; Gorelik, J.; Ostanin, V. P.; Lab, M. J.; Moss, G. W. J.; Frolenkov, G. I.; Klenerman, D.; Korchev, Y. E. *Nat. Methods* **2009**, *6*, 279–281.
- (30) Del Linz, S.; Willman, E.; Caldwell, M.; Klenerman, D.; Fernández, A.; Moss, G. *Anal. Chem.* **2014**, *86*, 2353–2360.
- (31) Seifert, J.; Rheinlaender, J.; Novak, P.; Korchev, Y. E.; Schäffer, T. E. *Langmuir* **2015**, *31*, 6807–6813.
- (32) Brown, K. T.; Flaming, D. G. *Advanced micropipette techniques for cell physiology*; John Wiley & Sons: New York, NY, 1986.
- (33) Yuill, E. M.; Shi, W.; Poehlman, J.; Baker, L. A. *Anal. Chem.* **2015**, *87*, 11182–11186.
- (34) Perry, D.; Momotenko, D.; Lazenby, R. A.; Kang, M.; Unwin, P. R. *Anal. Chem.* **2016**, *88*, 5523–5530.
- (35) Chowdhury, T. K. *J. Phys. E: Sci. Instrum.* **1969**, *2*, 1087–1090.
- (36) Ying, L. M.; Bruckbauer, A.; Rothery, A. M.; Korchev, Y. E.; Klenerman, D. *Anal. Chem.* **2002**, *74*, 1380–1385.
- (37) Caldwell, M.; Del Linz, S. J. L.; Smart, T. G.; Moss, G. W. J. *Anal. Chem.* **2012**, *84*, 8980–8984.
- (38) Novak, P.; Gorelik, J.; Vivekananda, U.; Shevchuk, A. I.; Ermolyuk, Y. S.; Bailey, R. J.; Bushby, A. J.; Moss, G. W. J.; Rusakov, D. A.; Klenerman, D.; Kullmann, D. M.; Volynski, K. E.; Korchev, Y. E. *Neuron* **2013**, *79*, 1067–1077.
- (39) Pellegrino, M.; Orsini, P.; Pellegrini, M.; Baschieri, P.; Dinelli, F.; Petracchi, D.; Tognoni, E.; Ascoli, C. *Micro Nano Lett.* **2012**, *7*, 317–320.
- (40) Terejanskzy, P.; Makra, I.; Fürjes, P.; Gyurcsányi, R. E. *Anal. Chem.* **2014**, *86*, 4688–4697.
- (41) Tognoni, E.; Baschieri, P.; Ascoli, C.; Pellegrini, M.; Pellegrino, M. *Micron* **2016**, *83*, 11–18.
- (42) Rheinlaender, J.; Geisse, N. A.; Proksch, R.; Schäffer, T. E. *Langmuir* **2011**, *27*, 697–704.
- (43) White, H. S.; Bund, A. *Langmuir* **2008**, *24*, 2212–2218.
- (44) Pellegrino, M.; Orsini, P.; Pellegrini, M.; Baschieri, P.; Dinelli, F.; Petracchi, D.; Tognoni, E.; Ascoli, C. *Neurosci. Res.* **2011**, *69*, 234–240.
- (45) Newman, J. J. *Electrochem. Soc.* **1966**, *113*, 501–502.
- (46) Hall, J. E. *J. Gen. Physiol.* **1975**, *66*, 531–532.
- (47) Pastré, D.; Iwamoto, H.; Liu, J.; Szabo, G.; Shao, Z. *Ultramicroscopy* **2001**, *90*, 13–19.
- (48) Shevchuk, A. I.; Gorelik, J.; Harding, S. E.; Lab, M. J.; Klenerman, D.; Korchev, Y. E. *Biophys. J.* **2001**, *81*, 1759–1764.
- (49) Thatenhorst, D.; Rheinlaender, J.; Schäffer, T. E.; Dietzel, I. D.; Happel, P. *Anal. Chem.* **2014**, *86*, 9838–9845.
- (50) Mann, S. A.; Hoffmann, G.; Hengstenberg, A.; Schuhmann, W.; Dietzel, I. D. *J. Neurosci. Methods* **2002**, *116*, 113–117.
- (51) Happel, P.; Dietzel, I. D. *J. Nanobiotechnol.* **2009**, *7*, 7.